# Femtosecond transillumination optical coherence tomography

**Michael R. Hee, Joseph A. Izatt, Joseph M. Jacobson, and James G. Fujimoto**

*Department of Electrical Engineering and Computer Science, Research Laboratory of Electronics, Massachusetts Institute of Technology, Cambridge, Massachusetts 02139*

**Eric A. Swanson**

*Lincoln Laboratory, Massachusetts Institute of Technology, Lexington, Massachusetts 02173*

Received February 10, 1993

We describe a new technique, femtosecond transillumination optical coherence tomography, for time-gated imaging of objects embedded in scattering media. Time gating is performed with a fiber-optic interferometer with femtosecond pulses and coherent heterodyne detection to achieve a 130-dB dynamic range. A confocal imaging arrangement provides additional spatial discrimination against multiply scattered light. By time gating ballistic photons, we achieve 125-$\mu$m-resolution images of absorbing objects in media 27 scattering mean free paths thick. We derive a fundamental limit on ballistic imaging thickness based on quantum noise considerations.

Optical imaging of biological tissue is attractive because optical radiation is nonionizing and spectroscopic information on tissue pathology may be obtained. For these reasons, transillumination breast imaging has become an active area of investigation as a possible alternative to mammography. Time- and spatially resolved optical imaging methods attempt to increase image resolution by discriminating against multiply scattered light. Spatially resolved methods, including confocal imaging,[1] optical heterodyning,[2] and spatially incoherent imaging techniques,[3] reject transmitted light having certain directionality or spatial coherence properties.

A short pulse of light propagating through tissue will be lengthened by multiple scattering. A shadowgram of hidden objects may be reconstructed by time gating the early-arriving least-scattered light from the later-arriving diffuse, or multiply scattered, light. Incoherent time-gating methods, including electronic,[4] streak camera,[5,6] and various nonlinear gating[7–9] techniques, do not require a uniform phase front across the entire detector aperture. In contrast, coherent time-gating methods detect only light with spatial and phase coherence. Coherent approaches are based on both traditional[10] and electronic[11] time-resolved holographic and interferometric[12] methods.

In this Letter we describe femtosecond transillumination optical coherence tomography, a novel coherent imaging technique for simultaneous time- and spatially resolved imaging in scattering media. Time-resolved photon migration is investigated for what is to our knowledge the first time with the use of coherent detection. The coherent portion of a pulse transmitted through a scattering medium is found to emerge in separate ballistic and diffuse components. Time-gated imaging of hidden objects is demonstrated by selection of only ballistic light. Imaging with ballistic light achieves high resolution; however, quantum noise and tissue damage thresholds fundamentally limit the detection of ballistic light to breast tissue samples thinner than ~4 mm. Purely spatially resolved ballistic imaging techniques are shown to be inferior to time-gated methods.

In transillumination optical coherence tomography, short-coherence-length light transmitted through a specimen is temporally resolved by interferometric detection. Short pulses (50 to 400 fs) at 830 nm are generated by an 80-MHz mode-locked Ti:$Al_2O_3$ laser and coupled into a fiber-optic Mach–Zehnder interferometer (Fig. 1). Light retroreflected from a reference delay mirror is recombined with temporally broadened light transmitted through the sample. Interference is observed only for the component of the transmitted pulse that is coherent with and temporally overlaps the reference pulse. The mode-locked Ti:$Al_2O_3$ laser was chosen because of its high output power and broad wavelength tunability; however, short-coherence-length cw sources may also be used.

In the sample path, a confocal imaging arrangement provides directional rejection of scattered and spatially incoherent photons by the single-mode fiber aperture.[13] The fiber coupling requirement is equiv-

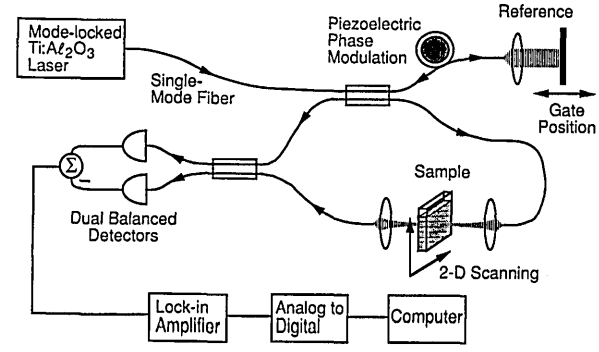


Fig. 1. Schematic of the fiber-optic transillumination optical coherence tomography system. 2-D, two dimensional.

0146-9592/93/120950-03$6.00/0 

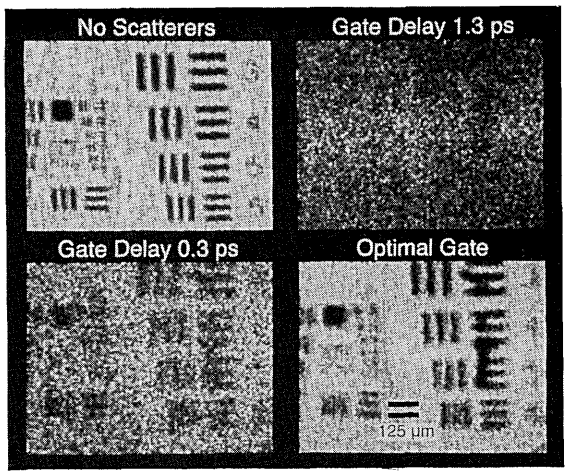


Fig. 2. Coherence-gated images of a resolution chart embedded in 27 scattering MFP's of 1-$\mu$m-diameter microspheres for various coherence-gate delays.

alent to the directional selection properties of spatially resolved imaging with an optical heterodyne receiver,[2] as well as spatially incoherent imaging techniques.[3]

The system can detect coherent transmitted light as small as $10^{-13}$ of the incident optical power of 45 mW. Heterodyne gain is produced by the interference of the strong reference beam with the weak signal beam emerging from the sample. A piezoelectric fiber stretcher phase modulates the interference signal at 10 kHz, and use of lock-in detection filters out the predominant $1/f$ mechanical noise. Dual balanced detectors are used to cancel random laser intensity fluctuations and achieve quantum shot-noise-limited detection.

We obtained two-dimensional images of objects embedded in scattering media by fixing the reference path length, or the coherence-gate delay, and measuring the magnitude of the interference signal while raster scanning the sample. A standard U.S. Air Force resolution chart was sandwiched between two 5-mm-long cuvettes containing 1-$\mu$m-diameter latex microspheres suspended in water. The optical thickness of the medium was 27 scattering mean free paths (MFP's) ($N\sigma L = \mu_s L = 27$, where $N = 1.9 \times 10^9$ cm$^{-3}$ is the number density, $\sigma = 1.4 \times 10^{-8}$ cm$^2$ is the scattering cross section computed from Mie theory, $\mu_s = 26.7$ cm$^{-1}$ is the scattering coefficient, and $L = 1$ cm is the total thickness).

Figure 2 displays the time-gated bar-chart images for various coherence-gate delays. Each $130 \times 100$ pixel image covered an actual area of 6.5 mm $\times$ 5 mm and required an 11-min acquisition time. The total energy deposited per pixel was 2.3 mJ ($4 \times 10^6$ pulses at 0.56 nJ/pulse). The upper-left-hand image is a reference image of the test chart measured through water alone. The lower-right-hand image was obtained through the scattering suspension with an optimal coherence gate set to select only unscattered ballistic light. The 125-$\mu$m-wide group II, element 1 bars are resolved. With a slightly nonoptimal coherence gate (0.3-ps delay), the chart is degraded but still visible (lower-left-hand image). With a 1.3-ps gate delay, the image consists almost entirely of diffuse light, and no bars are resolved (upper-right-hand image).

To investigate coherent photon migration, we measured the temporal behavior of the transmitted pulse through uniform scattering media. A 5-mm-long cuvette containing various concentrations of 1-$\mu$m-diameter latex microspheres suspended in water was placed in the sample arm. Light leaving the single-mode fiber was focused by a 12-mm focal-length diode collimating objective into the center of the cuvette. We measured the time-resolved coherent scattering profiles by scanning the reference arm path length and detecting the interference signal.

Figure 3 shows the normalized magnitude of the interference signal versus the coherence-gate delay for increasing optical thickness, measured in the number of scattering MFP's computed from Mie theory. The delay is displayed in normalized units of $ct/nL$, where $t$ is the actual time delay, $c/n$ is the speed of light in the medium, and $L$ is the sample length. For readability, the interference signal amplitudes are normalized to the same peak height; however, the absolute magnitudes attenuate with increasing scatterer concentration. For relatively transparent suspensions (0 to 15 MFP's) the laser power was attenuated to prevent detector saturation. Without attenuation, self-phase modulation in the fiber optics produced a reduction in the coherence length.

According to Fig. 3, the coherence-gated transmitted light consists of an unscattered ballistic

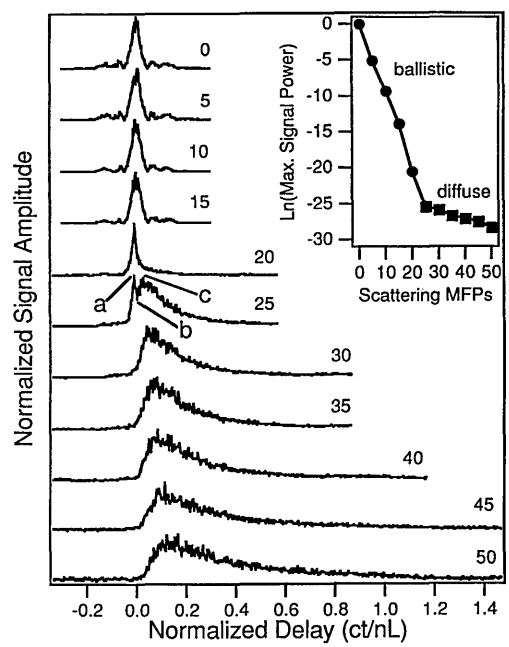


Fig. 3. Time-resolved scattering profiles of coherent photon migration through various concentrations of 1-$\mu$m-diameter microspheres. Linear plot of normalized interference signal magnitude versus normalized coherence-gate delay for concentrations of microspheres ranging from 0 to 50 MFP's. Points a, b, and c relate the coherence-gated images in Fig. 2 to a specific normalized delay on the time-resolved scattering profiles. Inset: attenuation of ballistic (circles) and diffuse (squares) peak powers obtained from the scattering profiles.

component and a temporally broadened diffuse component. The diffuse component contains the fraction of multiply scattered light that retains enough spatial and phase coherence to permit both confocal and coherent detection, respectively. The profiles demonstrate that a substantial amount of late-arriving light is coherent for samples thicker than 20 MFP's. The division into ballistic and diffuse components is qualitatively similar to earlier studies of time-resolved scattering with incoherent-gating techniques.[14,15] The points a, b, and c in Fig. 3 correspond to the normalized delay where the resolution chart images of Fig. 2 were obtained. Imaging of the ballistic light only (point a) results in theoretically diffraction-limited images, while selecting increasingly later diffuse light (points b and c) leads to progressively reduced image resolution.

The inset of Fig. 3 shows the exponential attenuation of the ballistic and diffuse peaks versus an increasing number of scattering MFP's, or equivalent sample thickness. The transmitted ballistic component attenuates by $1/e$ for every additional scattering MFP. This exponential decay with sample thickness implies that ballistic imaging may be performed only through relatively thin samples. A fundamental limit on both coherent and incoherent ballistic imaging through turbid media may be established by noting that the ballistic light must be detectable above the quantum shot-noise limit. For the case of perfect detector quantum efficiency, this limit is described by

$$L_{\text{ballistic}} = \frac{1}{\mu_t} \ln\left(\frac{1}{2}\frac{E}{h\nu}\right), \tag{1}$$

where a signal-to-noise ratio of one has been assumed as the detectivity limit, $L_{\text{ballistic}}$ is the maximum sample thickness, $\mu_t$ is the total attenuation coefficient (equal to the sum of the absorption and scattering coefficients), $E$ is the total optical energy delivered per spatial resolution element during detection, and $h\nu$ is the photon energy.

Tissue optical damage thresholds limit the maximum intensity that may be delivered to each pixel during detection, establishing a maximum ballistic imaging sample thickness through Eq. (1) of $\mu_t L \approx$ 36 MFP's.[16] For applications in early breast cancer diagnosis, the MFP's for both fatty and fibroglandular breast tissue are typically less than 100 $\mu$m,[17,18] defining a maximum ballistic imaging thickness of ~4 mm. Linear increases in optical power, data acquisition time, and number of averages affect only the maximum thickness as the logarithm and do not alter the limit appreciably.

Ballistic imaging with pure spatial discrimination techniques is further limited because a substantial amount of diffuse light may still be spatially coherent at the detector even when significant scattering has occurred. According to Fig. 3, high-resolution imaging with the use of spatially resolved methods is limited to the regime in which the ballistic component intensity overwhelms the delay-integrated diffuse component intensity, i.e., to specimens thinner than ~15–20 scattering MFP's (less than ~2 mm of breast tissue) for this imaging geometry.

Since ballistic imaging with any optical imaging technique is fundamentally limited by quantum noise to thin tissue samples, a practical time-domain imaging system must rely on the gating of early-arriving diffuse light. The inset of Fig. 3 shows that, compared with ballistic light, the transmitted coherent diffuse component attenuates by approximately a factor of 10 more slowly in the exponential with sample thickness. Thus early-arriving diffuse-light gated images should be possible through tissues of the order of centimeters thick.

We thank D. Huang for helpful scientific discussions. This research is supported in part by the National Institutes of Health (contract R0I GM35459-08) and the Medical Free Electron Laser Program (contract N00014-91-C-0084).

## References

1. D. S. Dilworth, E. N. Leith, and J. L. Lopez, Appl. Opt. **29,** 691 (1990).
2. M. Toida, M. Kondo, T. Ichimura, and H. Inaba, Appl. Phys. B **52,** 391 (1991).
3. E. N. Leith, C. Chen, H. Chen, Y. Chen, J. Lopez, P.-C. Sun, and D. Dilworth, Opt. Lett. **16,** 1820 (1991).
4. S. Andersson-Engels, R. Berg, S. Svanberg, and O. Jarlman, Opt. Lett. **15,** 1179 (1990).
5. J. C. Hebden, R. A. Kruger, and K. S. Wong, Appl. Opt. **30,** 788 (1991).
6. K. M. Yoo, B. B. Das, and R. R. Alfano, Opt. Lett. **17,** 958 (1992).
7. L. Wang, P. P. Ho, C. Lui, and G. Zhang, Science **253,** 769 (1991).
8. K. M. Yoo, Q. Xing, and R. R. Alfano, Opt. Lett. **16,** 1019 (1991).
9. M. D. Duncan, R. Mahon, L. L. Tankersley, and J. Reintjes, Opt. Lett. **16,** 1868 (1991).
10. K. G. Spears, J. Serafin, N. H. Abramson, X. Zhu, and H. Bjelkhagen, IEEE Trans. Biomed. Eng. **36,** 1210 (1989).
11. E. Leith, C. Chen, H. Chen, D. Dilworth, J. Lopez, J. Rudd, P.-C. Sun, J. Valdmanis, and G. Vossler, J. Opt. Soc. Am. A **9,** 1148 (1992).
12. D. Huang, E. A. Swanson, C. P. Lin, J. S. Schuman, W. G. Stinson, W. Chang, M. R. Hee, T. Flotte, K. Gregory, C. A. Puliafito, and J. G. Fujimoto, Science **254,** 1178 (1991).
13. M. Gu, C. J. R. Sheppard, and X. Gan, J. Opt. Soc. Am. A **8,** 1755 (1991).
14. K. M. Yoo and R. R. Alfano, Opt. Lett. **15,** 320 (1990).
15. Y. Kuga, A. Ishimaru, and A. P. Bruckner, J. Opt. Soc. Am. **73,** 1812 (1983).
16. With 800-nm light, the maximum permissible exposure for skin is $1.7t^{1/4}$ J cm$^{-2}$, where $t$ is the pulse-train exposure duration in seconds [ANSI Z136 (American National Standards Institute, 1986)]. Assuming a scanned 100 × 100 pixel image, 10-min total acquisition time, and 500-$\mu$m spatial resolution, the maximum energy $E$ permitted per pixel is 2.1 mJ.
17. W. Cheong, S. A. Prahl, and A. J. Welch, IEEE J. Quantum Electron. **26,** 2166 (1990).
18. H. Key, E. R. Davies, P. C. Jackson, and P. N. T. Wells, Phys. Med. Biol. **36,** 579 (1991).